IJISET - International Journal of Innovative Science, Engineering & Technology, Vol. 4 Issue 9, September 2017
ISSN (Online) 2348 – 7968 | Impact Factor (2016) – 5.264
www.ijiset.com

The Integration of ASTER Imagery and Airborne Gamma-ray Spectrometry in Lithological Discrimination of Ras Barud - Um Tagher Area, North Eastern Desert, Egypt

Dawoud, M.*; Abdel Ghani, I.M.; Elsaid, M.**; Badr, Y.S.****

* Geology Department, Faculty of Science, Menoufiya University

** Nuclear Materials Authority, P.O. Box 530, Maadi, Cairo, Egypt

1. Abstract

The present study aims at integrating the ASTER (VNIR+SWIR) data and airborne gamma-ray spectrometry to discriminate and mapping lithological units of Ras Barud - Um Tagher area, North Eastern Desert, Egypt. The study area is a part of the Arabian Nubian shield and comprises different crystalline basement rocks mainly represented by the intrusive rocks (Egyptian older and younger granites and younger gabbros) that intruded in the country rocks (metasediments). ASTER image processing techniques (color band composite (CBC) and principal component analysis (PCA)) highlighted subtle spectral variations between rock units and facilitating geological mapping of them. In addition, the radioelement composite image combines (K%, eTh and eU) in RGB delineates the lithological varieties with limited degree relative to the ASTER imagery. The field verification and petrographic investigation confirm the above-mentioned results of ASTER imagery and airborne gamma-ray spectrometry proposing a geological map (scale 1:50000) with an overall accuracy 84.63 % with a kappa coefficient value of 0.812.

Key words:

ASTER, Airborne gamma-ray spectrometry, Eastern Desert, Egypt, Ras Barud-Um Tagher, CBC, OIF, PCA, Geological mapping

2. Introduction

Advanced Spaceborne Thermal Emission and Reflection Radiometer (ASTER) is a Japanese satellite borne optical sensor equipped with 14 bands from the visible to near infrared (VNIR), shortwave infrared (SWIR) and thermal infrared (TIR) wavelength regions. The ASTER band divided into 3 VNIR, 6 SWIR and 5 TIR spectral bands. The six-spectral bands of ASTER

shortwave infrared (SWIR) radiation subsystem were designed to measure reflected solar radiation to distinguish Al–OH, Fe-O, Mg–OH, Si–O–H and CO_3 absorption features (Abrams and Hook, 1995; Fujisada, 1995). ASTER data has been used extensively in the last decade for geological mapping and mineral exploration because of the high spectral characteristics and low cost (Mars and Rowan, 2006; Rowan et al., 2006; Di Tommaso and Rubinstein, 2007; Moore et al., 2008; Azizi et al., 2010; Bedini, 2011; Elsaid et al., 2014; Ghosh et al., 2016; Gürsoy & Kaya, 2017).

Airborne gamma-ray spectrometry has been used as a tool for lithological mapping for many decades and continues to be developed (IAEA, 2003). This paper examined and compared the capability of both image processing techniques on ASTER (VNIR-SWIR) data and airborne gamma-ray spectrometry on mapping lithological units in arid regions.

3. Study area

Ras Barud - Um Tagher Area is bounded by latitudes 26^o 39` 30``- $26^o$ 51` 30`` N and longitudes 33^o 29` 30`` - $33^o$ 46` 30`` E, covering a total exposure surface area of about 602.5 km^2 (**Fig.1**). The area is characterized by rugged topography with low to moderate relief, where the highest elevation point in the area is G. Ras Barud about (1446 m above sea level). The area has a dendritic drainage, arid and rainless in summer while flash floods occasionally occur in winter and spring. The weather in summer is very hot (temperature sometimes exceeds 50 ^{o}C) and very cold in winter (at night temperature comes below 0 ^{o}C). Few trees such as Sanameka and Acacia are scattered along the main wadis of the area.

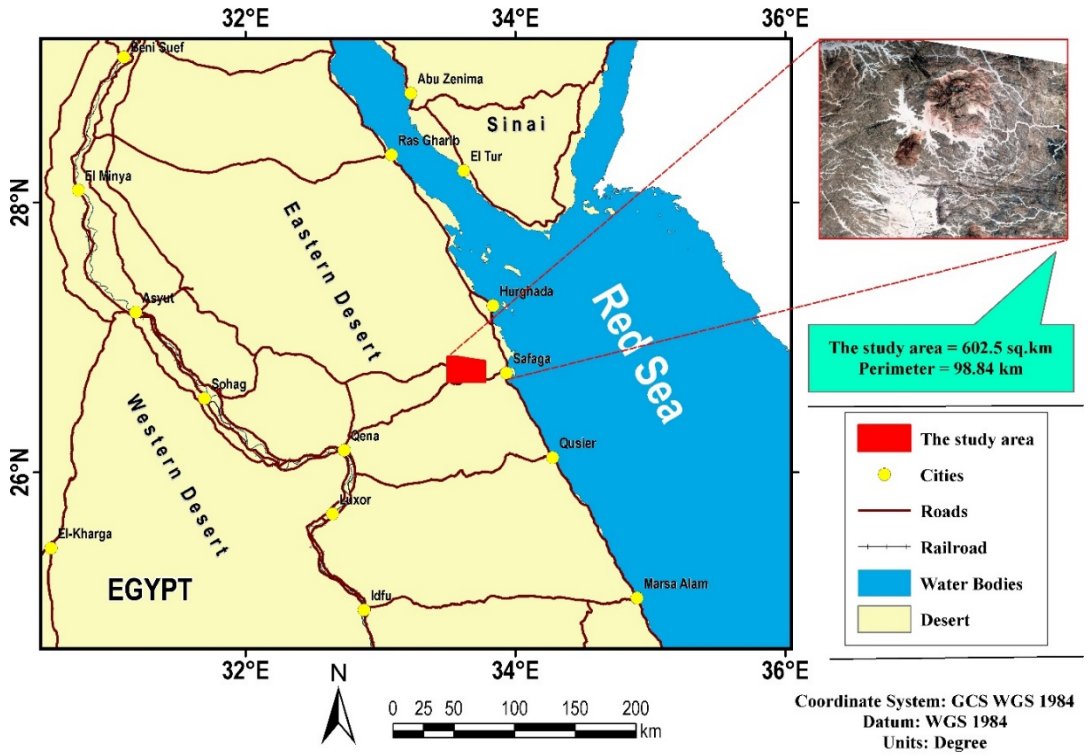

Fig.1: Location map of the study area

4. Data used and preprocessing

The ASTER L1B radiance at sensor scene covering the study area was acquired on Oct. 7th, 2007. The data were subsequently atmospherically-corrected using the Fast Line of-Sight Atmospheric Analysis of Spectral Hypercube (FLAASH). VNIR and SWIR bands were spatially resized to 30m x 30m pixels using nearest neighbor algorithm to preserve SWIR bands spectral characteristics (Galvão et al, 2005) using ENVI software. Furthermore, a geometric correction including orthorectification using ground control points and digital elevation model (SRTM v.3) was applied.

The airborne gamma-ray spectrometric data of the study area was acquired, in 1984. The survey was carried out along parallel flight lines oriented in a NE-SW direction at a 1.0 km spacing, while the tie lines were flown in a NW-SE direction at 10 km intervals at a nominal flight altitude of 120m terrain clearance (Aero-Service, 1984). The data generated from the flight line profiles were corrected for background radiation resulting from cosmic rays and aircraft contamination, for variations caused by changes in the aircraft altitude relative to the ground, and for Compton scattered gamma-rays in the potassium and uranium energy window. The data were prepared by digitizing the maps in numeric format by using Geosoft Oasis montage software.

5. Image processing and results

5.1. Color Band Composites (CBC)

Selection of better color composite for visual interpretation and lithological mapping of images was made using a statistical approach known as Optimum Index Factor (OIF). The Optimum Index Factor (OIF) is a statistic value that can be used to select the optimum combination of three bands in a satellite image with which you want to create a color composite. The optimum combination of bands out of all possible 3-band combinations is the one with the highest amount of 'information' (= highest sum of standard deviations), with the least amount of duplication (lowest correlation among band pairs) (Chavez et al., 1982). The optimum index factor was calculated using the following equation:

$$OIF = \frac{Si+Sj+Sk}{|Ri,j|+|Ri,k|+|Rj,k|}$$

Where;

S_i, S_j, and S_k are the standard deviations for bands i, j, and k, respectively,

$R_{i,j}$, $R_{i,k}$, and $R_{j,k}$ are the correlation coefficients between any two of the three bands being evaluated.

The best combination for lithological mapping is to be selected from the highest-ranking OIF calculated value. Bands 9, 8, 1 in RGB (**Fig.2**) represent the most informative color composite with highest OIF rank in the study area, highlighting differences between rock units and facilitating geologic mapping of them.

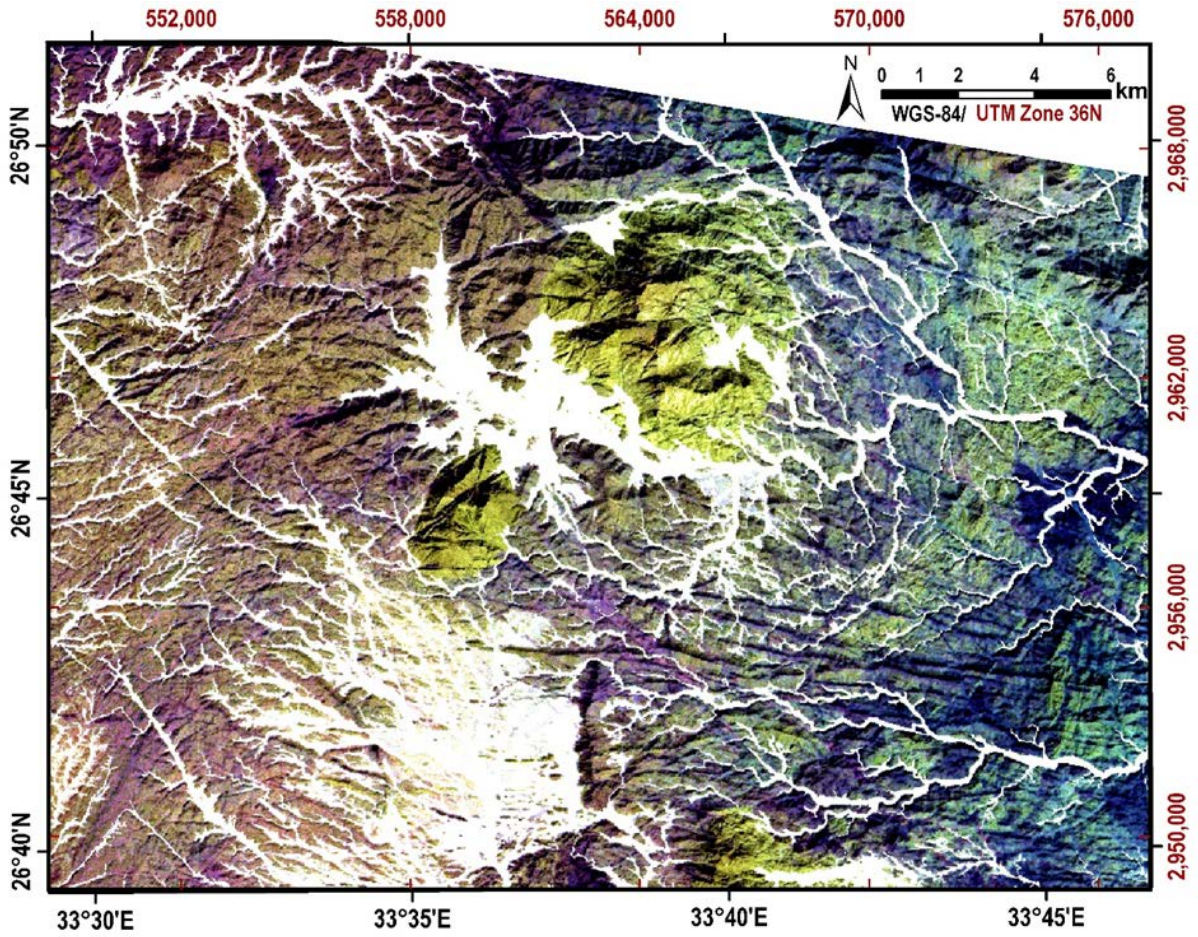

Fig.2: False color composite image bands 9,8, 1 in RGB

5.2. Principal component Analysis (PCA)

Principal component analysis (PCA) is a data transformation technique for simplifying a dataset by reducing multidimensional datasets to lower dimensions for analysis and for removing the redundancy of information that exists between the different bands to extract the relevant information from them **(**Loughlin, 1991; Gomez et al. 2005).

PCA was applied on ASTER (VNIR+SWIR) bands and the result was nine new image components were generated from the original input nine bands. PC1 describes the highest variance with positive loadings at each band **table (1).** PC1 concentrated features common to all input bands (usually topography) and displays important structural information. PC2 is orthogonal to PC1 in n directional space and highlighted the spectral differences between visible and the infrared spectral bands. PC3 is orthogonal to the other two PCs and includes the third most variability. After analyzing the eigenvalues of PC images, we realized that PC1, PC2, and PC3 contain the most variance of the data (99.57%).

The PCA eigenvalue plot of the VNIR + SWIR of ASTER data is shown in **Figure (3)**.

Table (1): Eigenvector values of principal component analysis (PCA) of the nine ASTER VNIR-SWIR bands.

PC	Band 1	Band 2	Band 3	Band 4	Band 5	Band 6	Band 7	Band 8	Band 9	Eigen value %
PC 1	0.266	0.310	0.349	0.383	0.319	0.307	0.330	0.312	0.404	**97.5**
PC 2	0.489	0.515	0.437	-0.102	-0.206	-0.200	-0.204	-0.204	-0.359	**1.81**
PC 3	0.007	-0.068	-0.180	0.667	0.195	-0.022	0.185	-0.070	-0.663	**0.26**
PC 4	0.153	-0.042	-0.108	0.294	0.317	-0.252	-0.269	-0.676	0.429	**0.12**
PC 5	-0.556	0.053	0.434	0.396	-0.312	-0.441	-0.110	0.129	0.148	**0.10**
PC 6	0.405	0.107	-0.531	0.200	-0.424	-0.404	0.119	0.306	0.229	**0.06**
PC 7	0.119	-0.301	0.249	-0.263	0.192	-0.521	0.666	-0.107	-0.029	**0.03**
PC 8	-0.121	0.124	-0.026	0.084	-0.553	0.366	0.487	-0.525	0.094	**0.03**
PC 9	0.405	-0.716	0.333	0.196	-0.311	0.196	-0.192	0.044	0.028	**0.02**

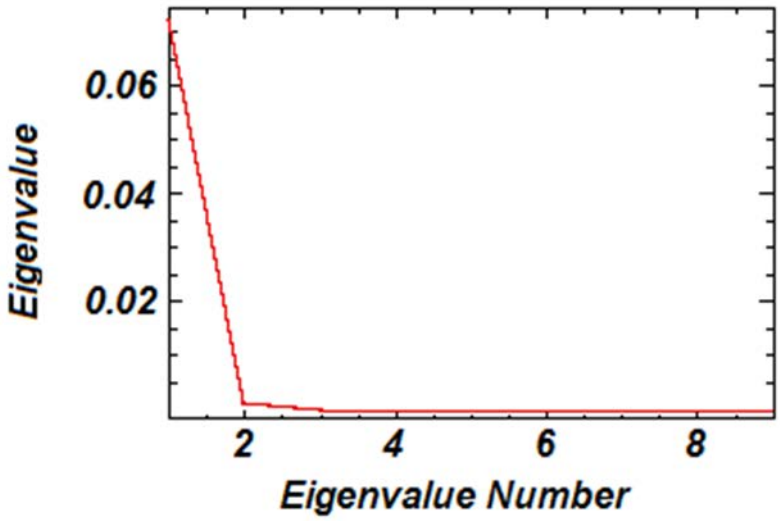

Fig.3: The PCA eigenvalue plot for the VNIR + SWIR bands of ASTER data

False Color Composite (FCC) image was generated using the three PCA outputs, including PC3, PC2 and PC1 giving the most informative (crisper) false color composite highlighting different lithological units along with structural features of the study area (**Fig.4**).

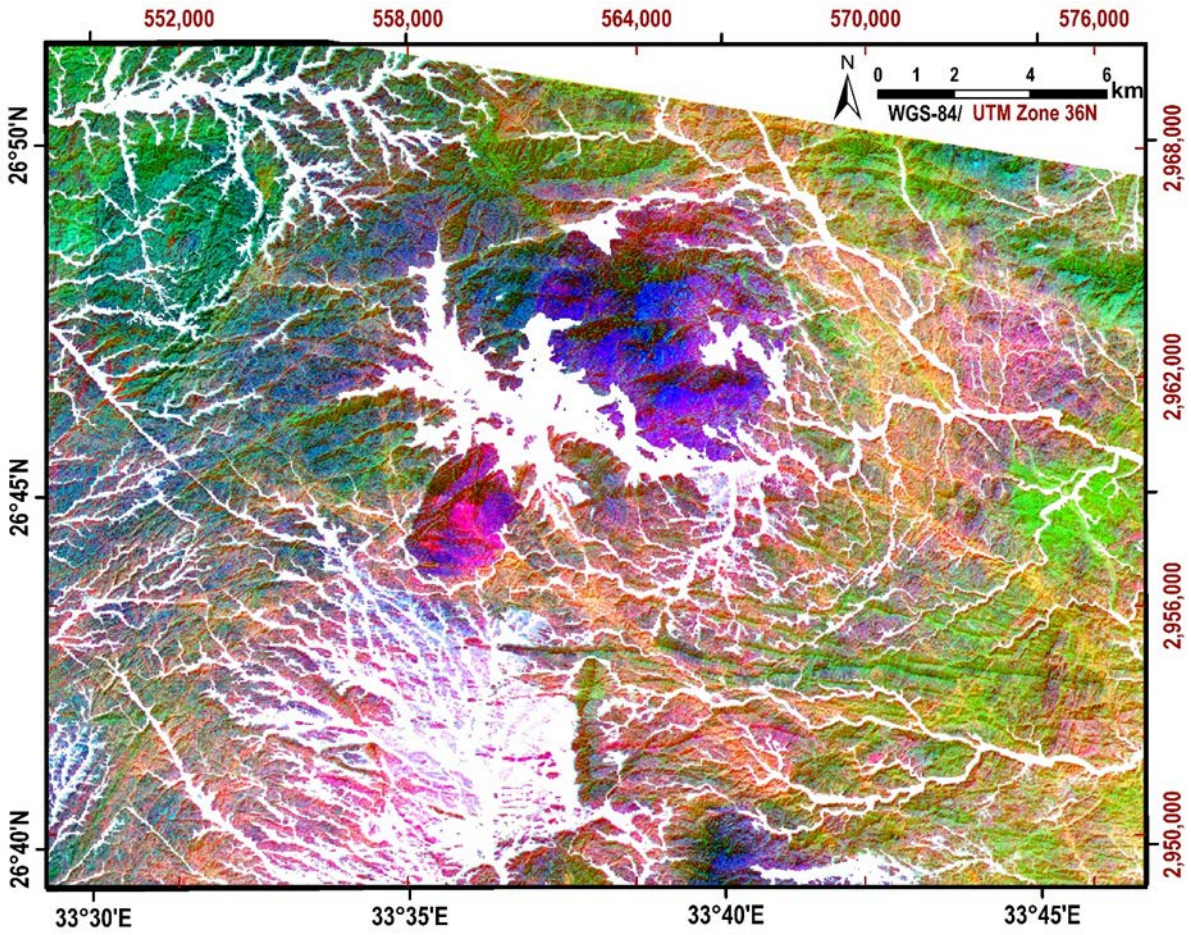

Fig.4: False color composite image of PCs (3, 2, 1 in RGB) using the nine ASTER VNIR-SWIR bands.

5.3. Radioelements composite image

The radioelement composite image map (**Fig.5**) combines the data K, eTh and eU in RGB. From the map, it is observed that the high concentration of K, eTh and eU (white color) is greatly correlated with the exposure of the younger granites rock unit. In addition, a small area of older granitoids (occurred at the southeastern part of the map covered by G. Ras Abda and an unmappable area at the east of G. Um Tagher El Foqani) also exhibit high concentration of K, eTh and eU.

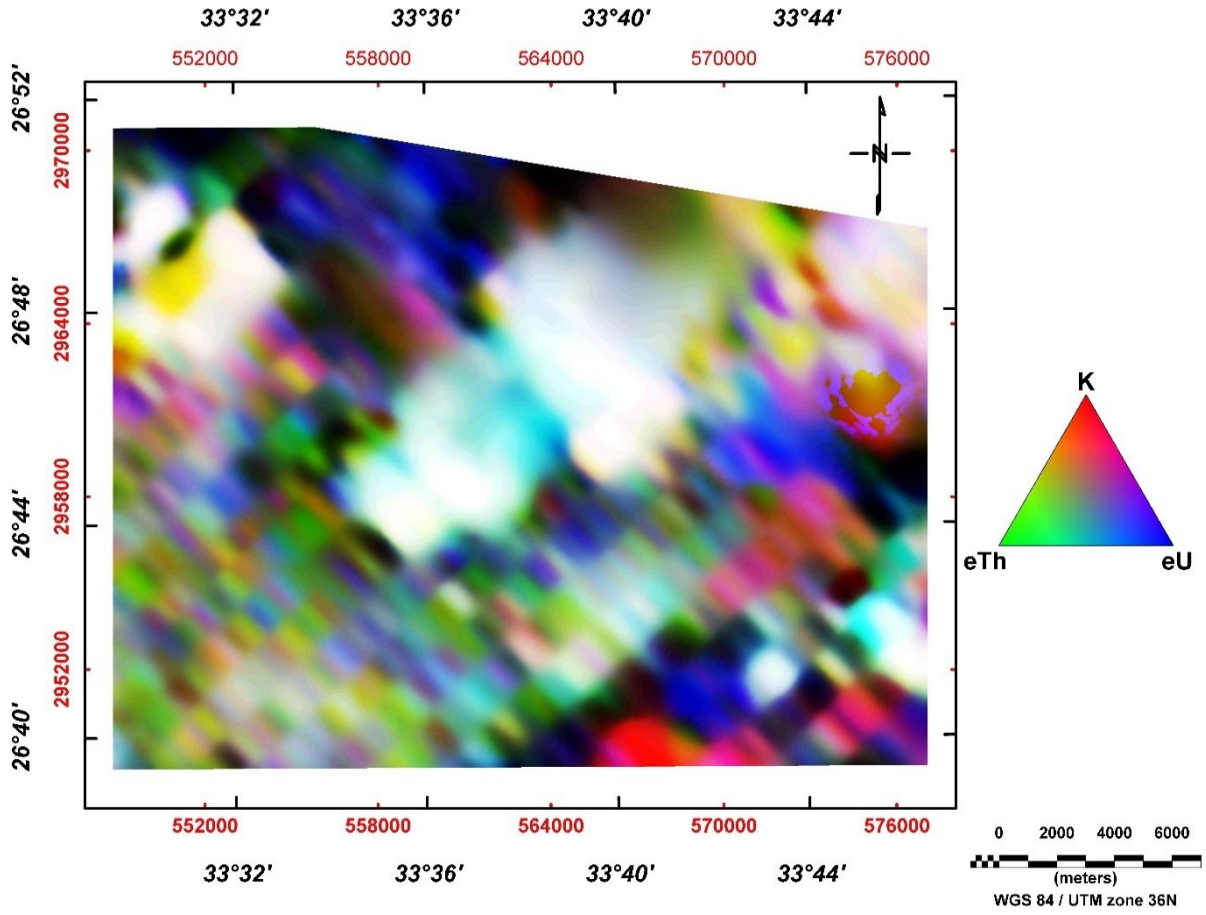

Fig.5: Radioelement composite image of K (in red), eTh (in green) and eU (in blue) of Ras Barud-Um Tagher area, North Eastern Desert, Egypt

6. Field Work and Petrographic Investigation

The results of ASTER image processing have been verified through intensive fieldwork. Sixty-three samples representing the different rock units that are cropping out in the study area with great focusing on granitic rocks were collected to obtain comprehensive information of the study area. The focusing on granitic rocks was due to they represent the most predominant rock unit covering about (472.6) km2 (78.51%) of the mapped area. The field characteristics of the granitic rock are shown in **figure** (**6**).

Petrographic investigation of twenty-five thin sections, representing the older granitoids and younger granites, were selected for determining the volume percentage of the rock forming minerals in the studied rock types. **Table (2)** shows the mineral constituents of these granitic samples**.** According to the modal classification of (Streckeisen, 1976), the older granitoids plot in the tonalite and granodiorite fields, whereas the younger granites plot in the fields of monzogranite, syenogranite and alkali-feldspar granite (**Fig.7**).

Fig.6: Field photographs of the studied granitic rocks:

A. Sub-vertical jointing and blocky appearance in granodiorite looking N 240° east G. Abu Hawis.
B. Close up view of detached block of granodiorite enclosing an elongated amphibolite enclave and quartz veinlet cutting it.
C. Sharp intrusive contact between younger gabbros (YGB) and older granitoids (OGR), looking N360° at W. Abu Hadida.
D. Close up view showing two sets of joints nearly perpendicular to each other in tonalite.
E. Panoramic view showing, G. Um Tagher El Foqani, G. Ras Barud and G. Abu Hawis.

Table.2: Modal analysis of the studied granitic rocks of Ras Barud - Um Tagher area

Rock type		S. No.	Mineral Constituents				
			Alkali-feldspars	Plag.	Quartz	Mafic	Acces.
Older granitoids	Tonalites	C4	1.7	58.3	22.2	14.2	3.6
		C13	2	49.4	29	16.3	3.3
		22	1.5	56	23.2	16.5	2.8
		C11	1.9	53.5	28	14.4	2.2
	Granodiorites	C6	12.5	52.7	22.9	9.3	2.6
		C2	14.1	48.9	25.3	8.6	3.1
		70	16	45.6	30.2	6.1	2.1
		31	15.3	49.4	27.5	5.9	1.9
		29	17.3	46.5	27.4	7.5	1.3
Statistics	Average		9.1	51.1	26.2	11.0	2.5
	Min.		1.5	45.6	22.2	5.9	1.3
	Max.		17.3	58.3	30.2	16.5	3.6
Younger granites	Monzogranites	28	30.2	27.4	35.8	4.6	2.0
		63	25.6	32.3	34.3	5.5	2.3
		T1	26.4	27.5	39.4	4.8	1.9
		T2	28.1	29	36.3	4.4	2.2
		35	21	34.6	38.9	4	1.5
		34	20.2	36.1	37.4	4.7	1.6
		C10	38	26.9	30.1	4.3	0.7
		C17	36.1	25.7	32.3	4.6	1.3
	Syenogranites	C8	56.1	8.3	31.6	3	1
		C9	59.3	6.9	30.7	2.68	0.42
		90a	45.5	17.8	33.4	2.3	1
		59	47	16.7	32.5	3	0.8
		90b	49.1	18.1	31.5	1.3	----
		C15	46.3	16.8	33.1	3.8	----
	Alkali-feldspar granites	C14A	66.5	2.9	27.5	2.48	0.62
		C14B	66.3	2.5	28	2.56	0.64
		61	63.7	1.1	32.5	1.7	1
		27	64.2	1.8	31.3	1.4	1.3
Statistics	Average		43.87	18.47	33.14	3.39	1.13
	Min.		20.2	1.1	27.5	1.3	----
	Max.		66.5	36.1	39.4	5.5	2.3

S. No = Sample number; Plag. = Plagioclase; Mafic (micas, chlorite and hornblende); Acces. = Accessories (zircon, apatite, allanite, sphene, …) and opaques; Min. = minimum; Max. = maximum.

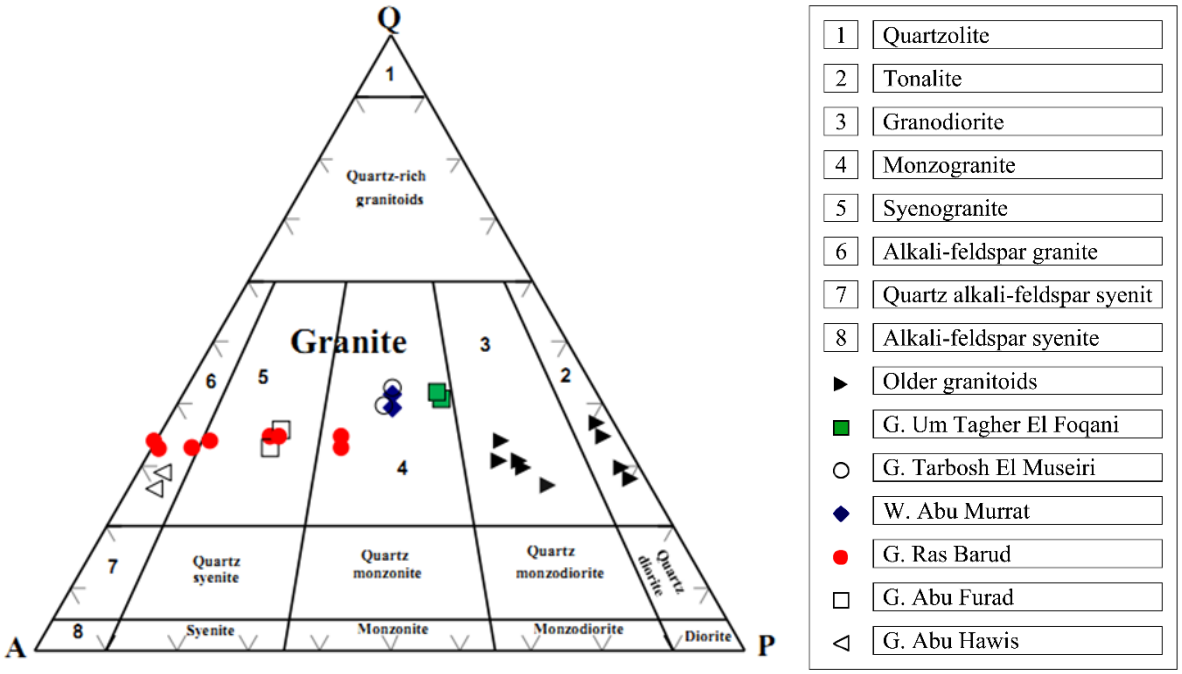

Fig.7: Q-A-P diagram according to the actual modal mineral constituents of Ras Barud - Um Tagher area granitic samples, (Streckeisen, 1976).

Depending on the results of ASTER image processing followed by extensive geologic field work and petrographic investigation, a geologic map (scale 1: 50,000) is constructed for Ras Barud - Um Tagher area (**Fig.8**).

A confusion matrix then applied using 100 ground truth areas randomly distributed and field checked over the study area representing all rock units to determine the overall accuracy of the proposed geological map. The overall accuracy found to be 84.63 % with a kappa coefficient value of 0.812.

7. Conclusions

ASTER (VNIR+SWIR) bands were examined to discriminate and mapping lithological unites of Ras Barud - Um Tagher area, North Eastern Desert, Egypt. The false color composite (B9, B8, B1 in RGB) showed limited enhanced visualization of the lithological units in the study area. Principal component analysis (PCA) used effectively in compressing the spectral information of the nine input VNIR-SWIR ASTR bands. The resulted first three PCs produced the most informative crisper false color composite (PC3, PC2, PC1 in RGB) highlighting the subtle spectral differences between different rock units within the study area. The younger granites are discriminated into, more or less, three lithological varieties while the younger gabbros are well discriminated. In

addition, the PCs discriminate the older granitoids from the adjacent lithological unites but could not differentiate them into well-defined varieties and this is in complete harmony with the fact of the complexity and heterogeneity of the older granitoids.

The field and petrographic investigations verified and confirmed the previously mentioned results and differentiated the younger granites into (alkali-feldspar granite, syenogranite and monzogranite) whereas the older granitoids are represented by tonalites and granodiorites. All results used in constructing a geological map with an overall accuracy of 84.63 % and a kappa coefficient of 0.812. Consequently, ASTER imagery processing is recommended as a rapid and cost effective multispectral data for mapping lithological units in arid regions.

The airborne gamma-ray spectrometric maps discriminate the younger granites in the area, but could not differentiate between their phases. The airborne gamma-ray spectrometry has a limited capability in discrimination and highlighting differences between rock units compared with ASTER imagery.

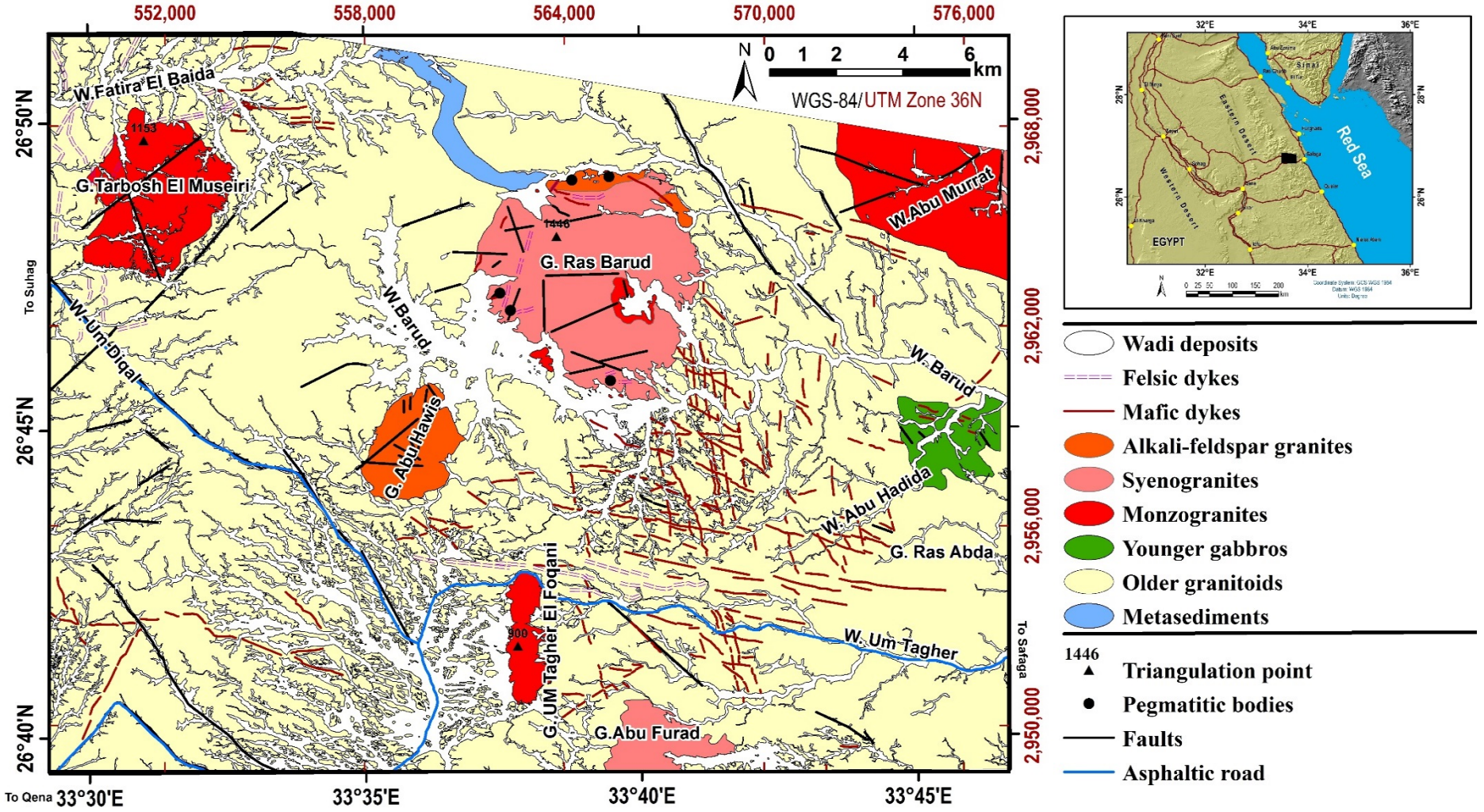

Fig.8: Geologic map of G. Ras Barud - Um Tagher area, North Eastern Desert, Egypt

8. References

Abrams, M., Hook, S.J., 1995: Simulated ASTER data for geologic studies. IEEE Trans. Geosci. Remote. Sens. 33 (3).

Aero Service, 1984: Final operational report of airborne magnetic/ radiation survey in the Eastern Desert, Egypt, for the Egyptian General Petroleum cooperation. Aero Service, Houston, Texas, April, 1984, six volumes.

Azizi, H., Tarverdi, M.A., Akbarpour, A., 2010: Extraction of hydrothermal Alterations form ASTER SWIR data from east Zanjan, northern Iran. Adv. Space Res. 46, 99–109.

Bedini, E., 2011: Mineral mapping in the Kap Simpson complex, central East Greenland, using HyMap and ASTER remote sensing data. Advance in Space Research 47, 60–73.

Chavez, P.S.J., Berlin ,G.L., Sowers, L.B., 1982: Statistical methods for selecting Landsat-MSS ratios. Journal of Applied Photogrammetric Engineering 8, 23-30.

Di Tommaso, I., Rubinstein, N., 2007: Hydrothermal alteration mapping using ASTER data in the infiernillo porphyry deposit, Argentina. Ore Geol. Rev. 32, 275–290.

Elsaid, M., Aboelkhair, H., Dardier, A., Hermas, E., 2014: Investigation of a relation between radiogenic heat production and kinetic surface temperature from multispectral ASTER-TIR data: a case study on Elmissikat-Eleridiya granites, Central Eastern Desert, Egypt. Arab J Geosci 7: 4615. doi:10.1007/s12517-013-1118-8.

Fujisada, H., 1995: Design and performance of ASTER instrument, in Breckinridge, J.B. (Ed.), Proceedings of International Society of Optical Engineering, vol. 2583, pp. 16–25.

Galvão, L. S., Almeida-Filho, R., and Vitorello, Í., 2005: Spectral discrimination of hydrothermally altered materials using ASTER short-wave infrared bands: Evaluation in a tropical savannah environment: International Journal of Applied Earth Observation and Geoinformation, v. 7, no. 2, p. 107-114.

Ghosh, U.K., Naik, K.K. & Kesari, M.P., 2016: Digital image processing of multispectral ASTER imagery for delineation of alteration and related

clay minerals in Sakoli belt: Maharashtra – A case study. J. Geol. Soc. India 88: 464. doi:10.1007/s12594-016-0509-3

Gomez, C., Delacourt C., Allemand, P., Ledru, P. Wackerle, R., 2005: Using ASTER remote sensing data set for geological mapping, in Namibia, Physics and Chemistry of the Earth 30, pp. 97–108.

Gürsoy, Ö. & Kaya, Ş., 2017: Detecting of Lithological Units by Using Terrestrial Spectral Data and Remote Sensing Image. J Indian Soc Remote Sens, 45: 259. doi:10.1007/s12524-016-0586-1

International Atomic Energy Agency, 2003: Guidelines for radioelement mapping using gamma-ray spectrometry data: IAEA-TECDOC-1363, International Atomic Energy Agency, Vienna.

Loughlin, W. P., 1991: Principal Component Analysis for alteration mapping, Photogrammetric Engineering and Remote Sensing, v.57, pp.1163-1169.

Mars, J. C., and Rowan, L. C., 2006: Regional mapping of phyllic- and argillic- altered rocks in the Zagros magmatic arc, Iran, using Advanced Spaceborne Thermal Emission and Reflection Radiometer (ASTER) data and logical operator algorithms: Geosphere, v. 2, no. 3, p. 161-186.

Moore, F., Rastmanesh, F., Asady, H., Modabberi, S., 2008: Mapping miner-logical alteration using principal component analysis and matched filter processing in Takab area, north–west Iran, from ASTER data. Int. J. Remote Sens. 29 (10), 2851–2867.

Rowan, L.C., Robert, G.S., John, C., 2006: Distribution of hydrothermally altered rocks in the Reko Diq, Pakistan mineralized area based on spectral analysis of ASTER data. Remote Sens. Environ. 104, 74–87.

Streckeisen, A., 1976: Classification of the common igneous rocks by means of their chemical composition: a provisional attempt. N. Jb. Min. Jour., 1-15.